THE JOURNAL OF PHYSICAL CHEMISTRY C

Article

pubs.acs.org/JPCC

Vanadium Substitution of $LiFePO_4$ Cathode Materials To Enhance the Capacity of $LiFePO_4$-Based Lithium-Ion Batteries

Ching-Yu Chiang,[†,‡] Hui-Chia Su,*[,†] Pin-Jiun Wu,[†] Heng-Jui Liu,[§] Chih-Wei Hu,[†,∥] Neeraj Sharma,[⊥] Vanessa K. Peterson,[⊥] Han-Wei Hsieh,[#] Yu-Fang Lin,[#] Wu-Ching Chou,[‡] Chih-Hao Lee,[†,∥] Jyh-Fu Lee,[†] and Bor-Yuan Shew*[,†]

[†]National Synchrotron Radiation Research Center, Hsinchu 30076, Taiwan

[‡]Institute and Department of Electrophysics, National Chiao Tung University, Hsinchu 30010, Taiwan

[§]Department of Material Science, National Tsing Hua University, Hsinchu 30013, Taiwan

[∥]Department of Engineering and System Science, National Tsing Hua University, Hsinchu 30013, Taiwan

[⊥]Australian Nuclear Science and Technology Organisation, Locked Bag 2001, Kirrawee DC, NSW 2232, Australia

[#]Advanced Lithium Electrochemistry Company, Ltd., Taoyuan 33048, Taiwan

ABSTRACT: The mechanism of enhancing the capacity of the $LiFePO_4$ cathodes in lithium ion batteries by the addition of a small amount of vanadium, which locate on the lithium site and induce lithium vacancies in the crystal structure, is reported in this article. As a result, the capacity increases from 138 mAh/g found for pristine $LiFePO_4$ to 155 mAh/g for the V-added compound, and the conductivity increases from 4.75×10^{-4} S/cm for the $LiFePO_4$ without V addition to 1.9×10^{-2} S/cm for the V-added compound. A possible model to facilitate the enhancement of conductivity and capacity is described with evidence supported by X-ray powder diffraction, X-ray absorption spectroscopy, and neutron powder diffraction data.

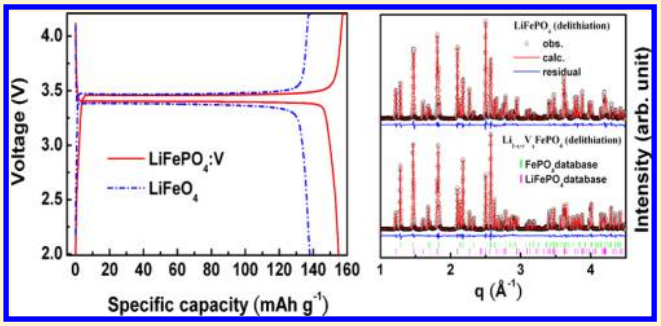

1. INTRODUCTION

Among the various cathode materials used in lithium ion batteries, lithium iron phosphate ($LiFePO_4$) has attracted great interest because of its environmental friendliness, low cost, long cycling life, and high specific energy.[1] Nevertheless, in order to compete with the electrochemical performances of other commercial cathode materials, such as $LiCoO_2$, $LiMnO_2$, etc., the capacity of $LiFePO_4$ needs to be significantly improved. The low capacity of pristine $LiFePO_4$ is due to the relatively low electronic conductivity and low diffusion rate of Li^+ ions within the structure, which limits the amount of Li^+ ions that can be extracted and hence limits the further commercial development of this material.[1,2] The electronic conductivity can be improved by coating a layer of carbon[3,4] and by adding transition metals.[5−10] In addition, the Li^+ ion diffusion rate and the amount of lithium extracted from $LiFePO_4$ can be manipulated by synthesizing nanometer grain sizes,[10,11] as well as by adding transition metals.[12−14] Therefore, in this work, to maximize electronic conductivity, minimize Li^+ ion diffusion lengths, maximize Li^+ ion diffusion rates in $LiFePO_4$ particles, the addition of transition metals to nanometer-sized $LiFePO_4$ is the most viable method. This scheme results in an improvement in both the capacity and electronic conductivity simultaneously. Although some reports of the surface coating of $LiFePO_4$ particles with metal oxides such as ZrO_2[15] and ZnO[16] demonstrated significant improvements in capacity retention, the enhancement is found to be lower than what is afforded by cation (transition metal) substitution into the $LiFePO_4$ crystal structure.

In this work, we will investigate the mechanism of improving the electrochemical properties of a pristine $LiFePO_4$ by fabricating nanometer sized cathodes with V incorporated into the $LiFePO_4$ crystal structure preferentially at the M1 site. In many previous studies, cationic substitution to the Fe site (M2 site) in $LiFePO_4$ usually results in higher ionic mobility and Li^+ diffusion coefficient as a result of the cell volume expansion and the probable weakening of the Li−O interactions.[13,14,17] The result can be named as pillar effect,[18,19] which supports the layered crystalline structure to avoid collapse during the lithiation and delithiation cycles. The weakening of the Li−O interactions lowers the charge transfer resistance and thus improves the reversibility of lithiation and delithiation also. However, only a limited number of reports[5,20] showed that cationic substitution to the Li site (M1 site) is probable, and it results in the production of Li vacancies that increases the capacity of $LiFePO_4$, which is significantly different to the pillar effect previous reported.

In the following, we will describe the evidence for (a) the vanadium substitution at the lithium (M1) site in the $LiFePO_4$

Received: July 16, 2012
Revised: October 22, 2012
Published: October 25, 2012

   dx.doi.org/10.1021/jp307047w | J. Phys. Chem. C 2012, 116, 24424−24429

crystal structure, (b) the mechanism of the conductivity and capacity enhancement, and (c) the electrochemical properties of charging and discharging rates from 0.2 to 20 C affected by the vanadium substitution effect. The experimental methods includes several techniques, such as X-ray powder diffraction (XRD), neutron powder diffraction (NPD), and X-ray absorption spectroscopy (XAS) including X-ray absorption near edge structure (XANES) and extended X-ray absorption fine structure (EXAFS) analysis. The investigation on the correlations between the structure and electrochemical properties will be reported in the following.

2. EXPERIMENTAL SECTION

Cathode materials consisting of $LiFePO_4$ with different concentrations of V_2O_5 were manufactured by Advanced Lithium Electrochemical Co., Ltd. (ALEEES) via a modified sol−gel process. The process used precursors of $LiOH{\cdot}H_2O$ (99.9%, Aldrich), $FeC_2O_4{\cdot}2H_2O$ (99%, Aldrich), and $NH_4{\cdot}H_2PO_4$ (97%, Aldrich), which were dissolved in deionized water. Stoichiometric quantities of V_2O_5 (99.9%, Aldrich) was added into the solution, followed by the addition of citric acid and mixing. The resulting suspension was mixed with 5 wt % sucrose and spray-dried using a hot air stream with an inlet pressure of 0.2 MPa. Inlet and outlet temperatures of the dryer were 220 and 100 °C, respectively. The powders were subsequently calcined at 800 °C for 12 h in a N_2 atmosphere and cooled to room temperature to yield the final product, $LiFePO_4$:V.

For the electrochemical tests, $LiFePO_4$:V was mixed with carbon black and polyvinylidene fluoride in a weight ratio of 85:8:7 to form the cathode material, and then assembled into a 2032-type coin cell with a lithium metal anode and 1 M lithium hexafluorophosphate in an ethylene carbonate/dimethyl carbonate solution as the electrolyte. The coin cell was assembled inside an argon-filled glovebox. Room-temperature galvanostatic cycling was carried out between 2.5 and 4.2 V at 0.2 C (where 1 C is equal to the charge of the battery in one hour). To understand the discrepancy of the discharging process at different C-rates, 18650-type cells were prepared to perform the measurements at various charging and discharging rates between 0.2 C (34 mAg^{-1}) and 20 C (3.4 Ag^{1-}). All electrochemical experiments were conducted under ambient conditions.

The crystal structures were determined by synchrotron XRD performed at beamlines BL01C2 and BL17A1 in the National Synchrotron Radiation Research Center (NSRRC), Taiwan. Further structural information was obtained using NPD, performed on the high-resolution powder diffractometer, Echidna,[21] in Australian Nuclear Science and Technology Organisation (ANSTO). The refinement of structural models with XRD and NPD data was based on the conventional Rietveld method using GSAS implemented with the EXPGUI interface.[22] XAS data were collected at the wiggler-equipped beamlines BL17C1, BL16A1, and BL07A1 in NSRRC.[23,24] Photon energies were calibrated to the V and Fe *K*-edge absorption energies. The data were analyzed by IFEFFIT-based program packages.[25] The pseudo radial structure function (RSF) for the central absorbing atom was obtained from Fourier transformation of the k^3-weighted EXAFS oscillations over the k range of 2.7−14.1 $Å^{-1}$. The V distribution inside $LiFePO_4$ nanoparticles was mapped by an energy dispersive spectrometer (EDS) under a high-resolution transmission electron microscope with lateral resolution of less than 0.2 nm.

3. RESULTS AND DISCUSSION

3.1. X-ray Powder Diffraction. XRD patterns of pristine $LiFePO_4$ and $LiFePO_4$:V samples are shown in Figure 1. The main peaks of all samples can be indexed to an orthorhombic olivine structure. In Figure 1, the pristine $LiFePO_4$ contains a Li_3PO_4 impurity phase (marked by a star), which might be formed from the excess Li during sample fabrication. The minor phase, LiV_2O_5 (marked by a cross) was also found in $LiFePO_4$:V samples when 5% V was added. The grain size of $LiFePO_4$ and $LiFePO_4$:V were estimated to be 71 and 77 nm, respectively, based on the Scherrer equation. In addition, the EELS mapping of the TEM data reveals that V is uniformly distributed in the $LiFePO_4$:V sample, which means that V is incorporated into the $LiFePO_4$ matrix without phase separation or segregation. Details of the structural parameters derived from XRD data are summarized in Table 1. The volume of the unit cell of $LiFePO_4$:V (291.45 $Å^3$) is slightly larger than pristine $LiFePO_4$ (291.3 $Å^3$). All crystal axes expand slightly after the addition of V atoms. We propose that adding V acts as a nucleation seed to help the crystalline growth and promotes the dissolution of the impurity phases. In both cases, we find full Fe occupancy at the M2 site, which implies that no Fe is replaced by V in the unit cell of $LiFePO_4$:V. Unfortunately, the occupancy of Li cannot be refined precisely from the XRD pattern due to the X-ray being insensitive to lithium. Therefore, XAS and NPD were also used together for further analysis.

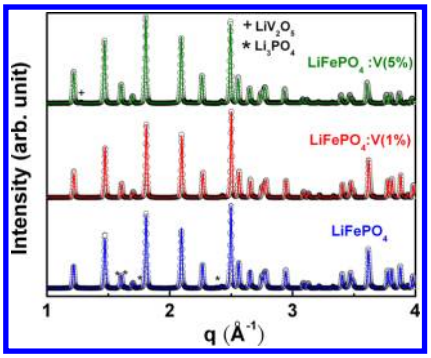

Figure 1. X-ray powder diffraction pattern of $LiFePO_4$, $LiFePO_4$:V(1%), and $LiFePO_4$:V(5%) with 12 keV X-rays and refined using $LiFePO_4$ models with GSAS. The star indicates the impurity phase of Li_3PO_4 in the pristine $LiFePO_4$ sample. The cross indicates the cluster-type phase of LiV_2O_5 in $LiFePO_4$:V(5%).

Table 1. Details Derived from the Rietveld Analysis Using X-ray Powder Diffraction Data of Pristine $LiFePO_4$, $LiFePO_4$:V(1%), and $LiFePO_4$:V(5%)

	lattice (*Pmnb*)					reliability factors		
sample	*a* (Å)	*b* (Å)	*c* (Å)	volume ($Å^3$)	Fe occup.	Rp (%)	Rwp (%)	χ^2
$LiFePO_4$	6.0074	10.3265	4.6957	291.298(8)	1	1.27	0.76	0.7400
$LiFePO_4$:V(1%)	6.0088	10.3292	4.6958	291.448(5)	1	1.25	0.61	0.6674
$LiFePO_4$:V(5%)	6.0022	10.3212	4.7015	291.256(5)	1	1.22	0.78	0.6610

dx.doi.org/10.1021/jp307047w | J. Phys. Chem. C 2012, 116, 24424−24429

3.2. X-ray Absorption Spectroscopy. The measured XANES and Fourier transformed EXAFS data of $LiFePO_4$:V at the V *K*-edge are shown in Figures 2 and 3. XANES is highly sensitive to the electronic structures around V; and EXAFS reveals the atomic structural characteristics around the local environments of V. The differential curves of the XANES data of $LiFePO_4$:V (1%) together with two standard reference samples, V_2O_3 and V_2O_5, are shown in the inset of Figure 2. In Figure 2, the pre-edge feature of V, which denotes the 1s → 3d quadruple transition due to a combination of stronger vanadium 3d−4p orbital coupling and the vanadium 3d orbitals hybridized with the oxygen 2p orbitals, is the most salient feature for determining the oxidation state of the absorbed atom and the symmetry of its surrounding environment. The white line indicates the dipole-allowed transition 1s → 4p. The reference V_2O_3 contains V in a distorted octahedral structure with three splitting 3d states, and the reference V_2O_5 contains V in a distorted square-pyramidal structure with only two split 3d states.[26] As shown in the inset of Figure 2, the differential curves reveal that the local structure of 1% V additive in $LiFePO_4$ is similar to the distorted octahedral structure found in V_2O_3 instead of the primitive square-pyramidal structure found in V_2O_5. XANES data reveals that 5% V additives in $LiFePO_4$ show different electronic configurations relative to 1% V additives, and thus the sample with 5% V additives is likely to be a complex mixture spectrum with V_2O_5 phase. From the chemical shift of the *K*-edge, the V additives exhibit an averaged oxidation state around 4^+. The ionic radius of V^{4+} in the octahedral coordination environment, determined by EXAFS, is about 0.72 Å, which is smaller than the radius of Li^+ (0.76 Å) and Fe^{2+} (0.78 Å) but much larger than P^{3+} (~0.4 Å). The P site has a feature of tetrahedral coordination environments and the small radius of P^{3+}, which are unlikely to be substituted by V. Moreover, the normalized peak intensity of the white line is larger than that of the references samples, which indicates emptier 4p states in the V-added samples and creates more positive holes to give rise to a p-type conductor behavior. From Figure 3, curves (a) and (e) show the fitted RSF of V and Fe *K*-edge with no phase correction for the $LiFePO_4$:V. The fitting parameters are summarized in Table 2. The curves (b), (c), and (d) are the calculated RSF of Li, P, and Fe for $LiFePO_4$, respectively, using the IFEFFIT-based program packages and with default Debye−Waller factors. From curves (a) and (e), the V and Fe core atoms have distinctly different RSF spectra in $LiFePO_4$:V, illustrating that the V and Fe atoms in $LiFePO_4$:V have different local surrounding environments. Comparing these five curves, the local environment of V in $LiFePO_4$:V samples is only similar to that of the lithium environment, suggesting that V is located at the Li (M1) site and not at the Fe (M2) or P sites, which is also consistent with the XRD and NPD data. Using the curves (a) and (b) in Figure 3, we observe that the bond length of the first shell of V is shorter than that of Li, implying that the next-nearest neighbor Li of $LiFePO_4$:V has a longer bond length of Li−O and weaker interactions with its surroundings.

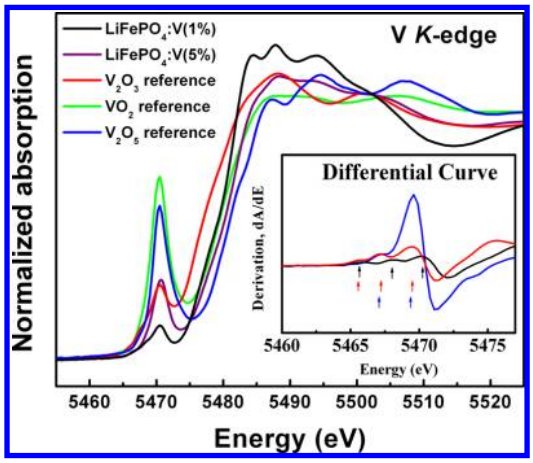

Figure 2. Normalized XANES spectra at the V *K*-edge of the $LiFePO_4$:V sample and compared with the spectral features of reference compounds. The inset shows the derivative curve of the pre-edge region, and the arrow indicates the *d* orbital splitting in the crystal field.

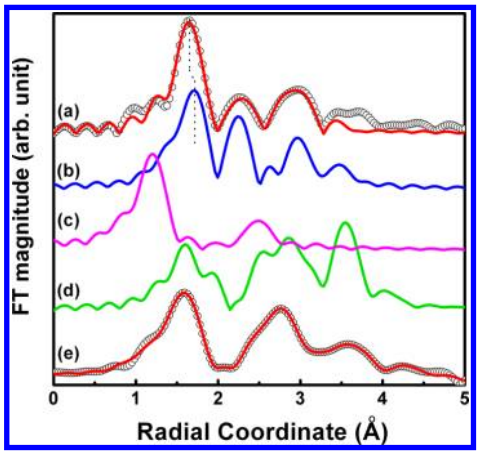

Figure 3. Fourier transformation of the k^3-weighted EXAFS oscillations at the V and Fe *K*-edge for the $LiFePO_4$:V sample (a), for V *K*-edge extended range and the fitting curve (b), the simulated spectrum for the Li environment, (c) the simulated spectrum for the P environment, (d) the simulated spectrum for the Fe environment, and (e) for Fe *K*-edge extended range and the fitting curve for $LiFePO_4$:V.

Table 2. Parameters of V and Fe *K*-Edge EXAFS Refinement for $LiFePO_4$:V

V *K*-edge			
path	deg × amp	σ_0^2	*R* (Å)
[O]	3.58	0.0018	2.022
[P]	1.71	0.0050	2.688
[P]	1.71	0.0020	3.232
[Fe]	6.61	0.0278	3.488
Fe *K*-edge			
path	deg × amp	σ_0^2	*R* (Å)
[O]	3.27	0.0076	2.053
[O]	1.26	0.0102	2.345
[P]	4.48	0.0151	2.952
[P]	1.97	0.0049	3.326
[Fe]	1.65	0.0061	3.9

3.3. Neutron Diffraction. NPD patterns of both $LiFePO_4$ and $LiFePO_4$:V samples are shown in Figure 4. Neutrons are generally more sensitive to the lighter elements than X-rays, and thus, careful Rietveld analysis was undertaken to compare pristine $LiFePO_4$ to $LiFePO_4$:V, and the pertinent details for the final models are listed in Table 3. NPD data sets were collected using the sample cans with the same size and for the same time on all samples, but the diffraction patterns are only subtly different. Similar structural parameters are derived from NPD as XRD data with respect to unit cell parameters and Fe

dx.doi.org/10.1021/jp307047w | J. Phys. Chem. C 2012, 116, 24424−24429

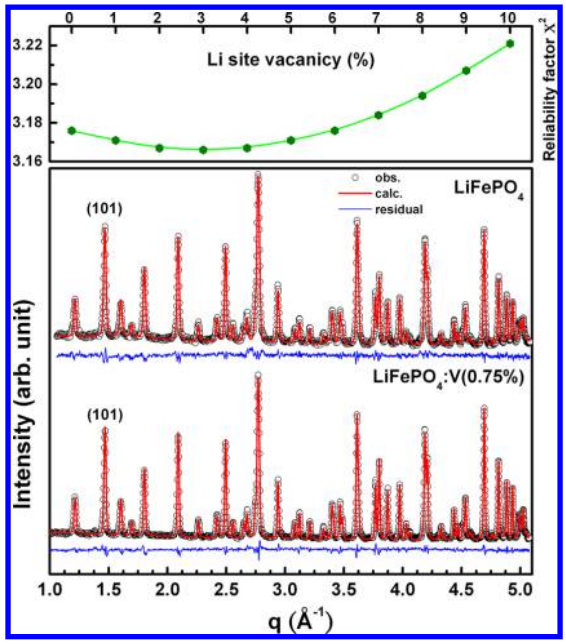

Figure 4. Goodness-of-fit term χ^2 variation relative to the percentage of Li site vacancy in $LiFePO_4$ structure after 0.75% vanadium addition derived from the fits to the neutron powder diffraction pattern $LiFePO_4$:V (the fit to $LiFePO_4$ is also shown).

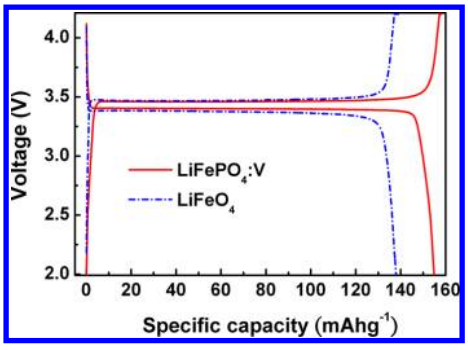

Figure 5. Charging/discharging curves of $LiFePO_4$:V and pristine $LiFePO_4$ cells over a voltage range of 2.0−4.2 V at a rate of 0.1 C.

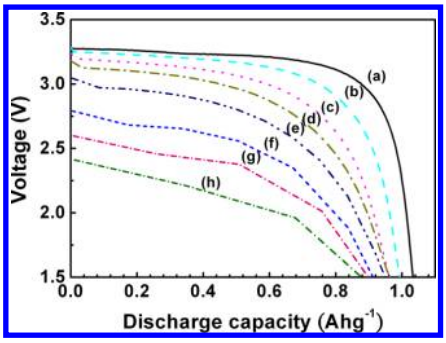

Figure 6. Discharging curves of 18650-type cell with $LiFePO_4$:V as the cathode material at the rate of (a) 0.2, (b) 0.5, (c) 1, (d) 2, (e) 5, (f) 10, (g) 15, and (h) 20 C.

occupancy on the M2 site. Furthermore, models with fixed lithium vacancies show better fits to the NPD data of the sample $LiFePO_4$:V. It is evident that V on the lithium site and lithium vacancies can be obtained by the Rietveld fits. We can quantitatively approximate that 3−4% Li vacancies (see Figure 4, top panel, goodness-of-fit term plotted as a function of Li vacancy) are created after 0.75% V added, which is consistent with the valence of V at about +4.

3.4. Electrochemical Performance Evaluation. Figure 5 shows the charging and discharging curves of pristine $LiFePO_4$ and $LiFePO_4$:V with 1% V additive within a voltage range of 2.0−4.2 V at 0.1 C. All charging and discharging profiles of these two samples exhibit flat operating voltages at about 3.45 V (charging) and 3.40 V (discharging). The separation between charging and discharging plateaus, also defined as the degree of polarization, of the $LiFePO_4$:V (51 mV) is significantly lower than that of the pristine $LiFePO_4$ (89 mV). This phenomenon means that Li^+ in $LiFePO_4$:V possess better insertion/extraction reversibility than in the pristine $LiFePO_4$. The specific capacity of $LiFePO_4$:V is 155 $mAhg^{-1}$, which is 12% larger than that of the pristine $LiFePO_4$ (138 mAh/g). The conductivity of $LiFePO_4$:V is also enhanced by a factor of 40 relative to the pristine $LiFePO_4$. The capacity during discharging at different C-rates is shown in Figure 6. A discharging capacity of 1.03 Ahg^{-1} was obtained at 0.2 C. As the C-rate increases from 0.2 to 20 C, the capacity decreases gradually but still remains at 0.88 Ahg^{-1} at 20 C. This result indicates good Li^+ extraction in $LiFePO_4$:V even when discharging at high C-rate. However, the enhanced electrochemical properties only appear substantially when the added V is less than 2%. It is interesting to further investigate the higher V concentration in impeding the Li diffusion rate in the future.

3.5. Model of V Substitution. Recently, vanadium incorporations into pristine $LiFePO_4$ had been noted and associated with improvements to the electrochemical performance of a lithium ion battery. Wen et al.[27] used Rietveld analysis of the XRD data to show that 1% V were randomly distributed at the Fe (M2) site in the $LiFePO_4$ structure and that there was improved electrochemical activity as a result of the V substitution. Yang et al.[17] reported 5% of Mg^{2+}, Ni^{2+}, Al^{3+}, or V^{3+} dopants at the Fe (M2) site and showed that a higher valence cation will result in a cathode exhibiting a larger specific discharge capacity. In their works, V substitution at the Fe site was determined by Rietveld analysis, and the valence of V was determined by the V *K*-edge XANES spectra. Sun et al.[12] prepared V-doped $LiFePO_4$/C powders through a carbothermal synthetic route expressing a higher Li^+ ion diffusion coefficient but a lower electrical conductivity. A higher discharge capacity of this sample relative the pristine $LiFePO_4$ was also noted, but the location of V in $LiFePO_4$ structure was determined. Hong et al.[28] used Rietveld analysis to show V at the P site in $LiFePO_4$ structure. Ma et al.[29] systemically investigated the additive ratio

Table 3. Details Derived from the Rietveld Analysis Using Neutron Powder Diffraction Data of Pristine $LiFePO_4$ and $LiFePO_4$:V(0.75%)

	lattice (*Pmnb*)					reliability factors		
sample	*a* (Å)	*b* (Å)	*c* (Å)	volume (Å^3)	Li occup.	Rp (%)	Rwp (%)	χ^2
$LiFePO_4$	6.0033	10.3199	4.6926	290.727(9)	1.000(13)	3.19	4.21	2.18
$LiFePO_4$:V(0.75%)	6.0046	10.3210	4.6923	290.797(6)	0.970(10)	3.75	4.86	3.166

dx.doi.org/10.1021/jp307047w | J. Phys. Chem. C 2012, 116, 24424−24429

dependence of the V-doped $LiFePO_4$ cathode. Their XRD data shows V^{4+} substitution at Fe site at lower concentrations (<7%), formation of nanosized VO_2 on the $LiFePO_4$ particle surface beyond the solid−solution limit, and formation of the secondary phase $Li_3V_2(PO_4)_3$ at higher concentrations (>11%). Zhang et al.[30] prepared $LiFe_{1-x}V_xPO_4$/C samples by using a two-step solid-state reaction. Their XANES results also determined the valence of V in $LiFe_{0.95}V_{0.05}PO_4$/C to be between +3 to +4. The above reports use Rietveld analysis of mostly XRD data to show the V location at the Fe site in the $LiFePO_4$ structure. However, it is difficult to precisely determine or model the location of a substituent atom at very low concentrations by Rietveld analysis using XRD data. EXAFS is a useful complementary technique to reveal the structural characteristics of $LiFePO_4$ as it is sensitive to the local environment around the absorbed atom. Zhao et al.[31] first showed that V was not at Fe nor P sites in their $LiFePO_4$ structure, but that V forms a $Li_3V_2(PO_4)_3$ secondary phase. Omenya et al.[32] showed the formation of the solid solution as a function of the synthesis temperature where at least 10 mol % of V^{3+} can be substituted at the Fe site in $LiFePO_4$ using appropriate temperatures. They showed that increasing the synthesis temperature to 700 °C leads to a decreased V solubility and the formation of a $Li_3V_2(PO_4)_3$ secondary phase. XANES and EXAFS indicated that V was in the 3^+ oxidation state in an octahedral environment at the Fe site in $LiFePO_4$. These results seem to contradict Zhao's reports. From the above descriptions, there is a lively debate in the literature over whether V atom substitution can be accomplished in the first place, but by extending these discussions one step further, our work is one of the studies to present that V substitutes at the Li (M1) site in $LiFePO_4$.

In our work, samples consist of V substituted at the Li site with approximately 3−4% vacancies, and we found no evidence for V clusters or impurity phases for $LiFePO_4$:V when the added V quantity is less than 2%. At higher concentrations, we note the formation of LiV_2O_5. The enhanced capacity and conductivity were observed when the V additive is less than 2%; hence, we focused our structural characterization on the region of the additive concentration of less than 2%. We find the similar enhanced electrochemical properties when V located at the Li site relative to the Fe site. Chung et al.[5] presented the benefits of aliovalent (Mg^{2+}, Al^{3+}, Ti^{4+}, Zr^{4+}, Nb^{5+}, or W^{6+}) substitution in the $LiFePO_4$ structure. They proposed that cation doping on the Li sites allows the stabilization of solid solutions with a net cation deficiency, although the site occupancy of specific dopants had yet to be established. In our work, we provide sufficient evidence that the generation of Li vacancies (ν'_{Li}) were induced after V addition at the Li site ($V^{\bullet\bullet\bullet\bullet}_{Li}$). Therefore, in the following, $LiFePO_4$:V samples are denoted as $Li_{1-x-\nu}V_xFePO_4$ to indicate that the added V is located at the Li site and that it created the vacancies of the Li sites. This argument is also supported by the work of Wagemaker et al.,[20] which showed that the aliovalent dopant charge is often balanced by the generation of Li vacancies. However, the immobile dopant within the Li channels slightly increases the size of the Li channels, which is still very limited to influence the Li-ion mobility and even hinder the Li-ion diffusion. From Wagemaker's report, it cannot explain how the cationic substitution into the Li site leads to a great enhancement of the electrochemical performance. Morgan et al.[33] reported that $FePO_4$ has lower activation barriers and a higher diffusion coefficient than $LiFePO_4$ by first-principles calculation. We proposed that Li ions can migrate easier via those excess Li vacancies. The following short equation (using Kröger−Vink notation[34]) describes the valence balance model:

$$\frac{1}{2}V_2O_5 \xrightarrow{LiFePO_4} V^{\bullet\bullet\bullet\bullet}_{Li} + \frac{5}{2}O^{\times}_{O} + 4\nu_{Li}' \quad (1)$$

Overall, Li^+ ions can move easier between the anode and the cathode through the increasing Li vacancy sites, which results in a decrease of polarization degree and enhanced the capacity and conductivity as we observe in the electrochemical measurements. The difference of the valence between original the Li atom and substituted V atom creates excess Li vacancies to balance the charge. However, a sample manufacturing process, which gives rise to different morphologies, might also play a critical role in the observed electrochemical properties.

3.6. Evolution of V with Lithiation and Delithiation.

The ex situ data of the lithiation and delithiation states provides the evidence of the structural changes of the $Li_{1-x-\nu}V_xFePO_4$ cathode during charging and discharging process. Th ex situ spectra were measured at the initial state (containing Fe^{2+}) and the delithiated state (containing Fe^{3+}) of $Li_{1-x-\nu}V_xFePO_4$ at 0.1 C. From the XANES data shown in Figure 7, it is obvious that

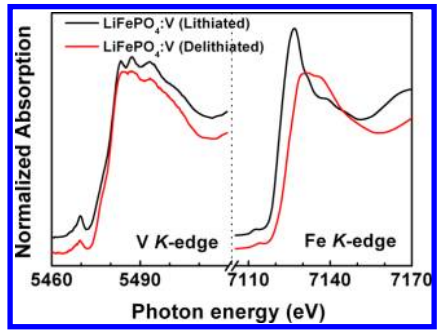

Figure 7. Ex situ normalized XANES spectra at V and Fe *K*-edge measured at the initial state (containing Fe^{2+}) and the delithiated state (containing Fe^{3+}) of $LiFePO_4$:V at 0.1 C.

the feature of Fe *K*-edge changed from Fe^{2+} to Fe^{3+} when charging to the delithiated state. However, the feature of V *K*-edge has no significantly changes from initial state to the delithiated state. The Fe *K*-edge curve revealed similar charging and discharging processes in $Li_{1-x-\nu}V_xFePO_4$ as in pristine $LiFePO_4$. From these data, we suggest that V remains at the Li site and is not electrochemically active even during the charging and discharging process. Otherwise, the V will redox if V substituted in

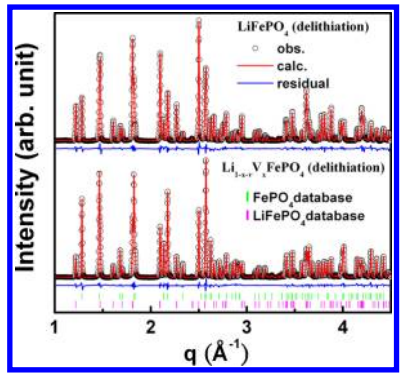

Figure 8. X-ray powder diffraction data of charged $LiFePO_4$ and $Li_{1-x-\nu}V_xFePO_4$ at 0.1 C and Rietveld-refined fit using $LiFePO_4$ and $FePO_4$ models.

dx.doi.org/10.1021/jp307047w | J. Phys. Chem. C 2012, 116, 24424−24429

the Fe site. The enhanced properties are correlated to the substitution of V at the Li site and the subsequent generation of Li vacancies. This result is also consistent with the reduced polarization voltage shown in Figure 5. In addition, from the ex situ XRD data of charged $LiFePO_4$ and $Li_{1-x-v}V_xFePO_4$, shown in Figure 8, the active Li^+ ions in $Li_{1-x-v}V_xFePO_4$ are greater in quantity than that of pristine $LiFePO_4$ by virtue of producing more $FePO_4$ in the former relative to the latter (see Table 4).

Table 4. Details Derived from the Rietveld Analysis Using ex Situ X-ray Powder Diffraction Data at Lithiation and Delithiation States of the Pristine $LiFePO_4$ and the $Li_{1-x-v}V_xFePO_4$ Samples

compound (delithiation)	$LiFePO_4$ volume (Å^3)	$FePO_4$ volume (Å^3)	mole ratio $FePO_4$/$LiFePO_4$
$LiFePO_4$	289.098(5)	269.810(8)	0.63
$Li_{1-x-v}V_xFePO_4$	288.878(7)	269.988(4)	1.84

This result also supports that the inactive lithium is reduced in this V-added composition

4. CONCLUSIONS

The investigation of the relationship between the enhanced electrochemical properties and the structure of $Li_{1-x-v}V_xFePO_4$ is described. By adding V_2O_5 into $LiFePO_4$ using a modified sol−gel synthesis process, better capacity and conductivity of $Li_{1-x-v}V_xFePO_4$ is found relative to pristine $LiFePO_4$. The enhanced properties are correlated to the substitution of V at the Li site and the subsequent generation of Li vacancies. The ex situ measurements also support this finding. The electrochemical performance shows that $Li_{1-x-v}V_xFePO_4$ can exhibit improved capacity not only at lower C-rate but also at higher C-rate.

AUTHOR INFORMATION

Corresponding Author

*(H.-C.S.) Tel: 886-3-5780281, ext. 6405. Fax: 886-3-5783805. E-mail: su.huichia@nsrrc.org.tw. (B.-Y.S.) Tel: 886-3-5780281, ext. 7316. Fax: 886-3-5783890. E-mail: yuan@nsrrc.org.tw.

Notes

The authors declare no competing financial interest.

ACKNOWLEDGMENTS

We would like to thank Mr. Cheng-An. Hsieh, Dr. Cheng-Yuan Cheng, and Dr. Wei-Tsung Chuang for experimental assistance and useful discussion. We also appreciate the comments from Drs. Mau-Tsu Tang, Hwo-Shuenn Sheu, and Jey-Jau Lee. Financial support was provided by Advanced Lithium Electrochemical Co., Ltd. (ALEEES).

REFERENCES

(1) Padhi, A. K.; Nanjundaswamy, K. S.; Goodenough, J. B. *J. Electrochem. Soc.* **1997**, *144*, 1188−1194.
(2) Andersson, A. S.; Thomas, J. O. *J. Power Sources* **2001**, *97*, 498−502.
(3) Wang, G. X.; Yang, L.; Bewlay, S. L.; Chen, Y.; Liu, H. K.; Ahn, J. H. *J. Power Sources* **2005**, *146*, 521−524.
(4) Park, K. S.; Kang, K. T.; Lee, S. B.; Kim, G. Y.; Park, Y. J.; Kim, H. G. *Mater. Res. Bull.* **2004**, *39*, 1803−1810.
(5) Chung, S. Y.; Bloking, J. T.; Chiang, Y. M. *Nat. Mater.* **2002**, *2*, 123−128.
(6) Herle, P. S.; Ellis, B.; Coombs, N.; Nazar, L. F. *Nat. Mater.* **2004**, *3*, 147−152.
(7) Croce, F.; Epifanio, A. D.; Hassoun, J.; Deptula, A.; Olczac, T.; Scrosati, B. *Electrochem. Solid-State Lett.* **2002**, *5*, A47−A50.
(8) Wang, G. X.; Bewlay, S.; Yao, J.; Ahn, J. H.; Dou, S. X.; Liu, H. K. *Electrochem. Solid-State Lett.* **2004**, *7*, A503−A506.
(9) Gouveia, D. X.; Lemos, V.; de Paiva, J. A. C.; Souza Filho, A. G.; Mendes, F. *Phys. Rev. B* **2005**, *72*, 024105.
(10) Yamada, A.; Chung, S. C.; Hinokuma, K. *J. Electrochem. Soc.* **2001**, *148*, A224−A229.
(11) Prosini, P. P.; Carewska, M.; Scaccia, S.; Wisniewski, P.; Passerini, S.; Pasquali, M. *J. Electrochem. Soc.* **2002**, *149*, A886−A890.
(12) Sun, C. S.; Zhou, Z.; Xu, Z. G.; Wang, D. G.; Wei, J. P.; Bian, X. K.; Yan, J. *J. Power Sources* **2009**, *193*, 841−845.
(13) Wang, D.; Li, H.; Shi, S.; Huang, X.; Chen, L. *Electrochim. Acta* **2005**, *50*, 2955−2958.
(14) Wang, C.; Hong, J. *Electrochem. Solid-State Lett.* **2007**, *10*, A65−A69.
(15) Liu, H.; Wang, G. X.; Wexler, D.; Wang, J. Z.; Liu, H. K. *Electrochem. Commun.* **2008**, *10*, 165−169.
(16) León, B.; Pérez Vicente, C.; Tirado, J. L.; Biensan, P.; Tessierb, C. *J. Electrochem. Soc.* **2008**, *155*, A211−A216.
(17) Yang, M. R.; Ke, W. H. *J. Electrochem. Soc.* **2008**, *155* (10), A729−A732.
(18) Liu, H.; Cao, Q.; Fu, L. J.; Li, C.; Wu, Y. P.; Wu, H. Q. *Electrochem. Commun.* **2006**, *8*, 1553−1557.
(19) Nakamura, T.; Miwa, Y.; Tabuchi, M.; Yamada, Y. *J. Electrochem. Soc.* **2006**, *153*, A1108−A1114.
(20) Wagemaker, M.; Ellis, B. L.; Dirk, L. H.; Mulder, F. M.; Nazar, L. F. *Chem. Mater.* **2008**, *20*, 6313−6315.
(21) Liss, K. D.; Hunter, B. A.; Hagen, M. E.; Noakes, T. J.; Kennedy, S. J. *Phys. B* **2006**, *385*−*386*, 1010−1012.
(22) Toby, B. H. *J. Appl. Crystallogr.* **2001**, *34*, 210−213.
(23) Tsang, K. L.; Lee, C. H.; Jean, Y. C.; Dann, T. E.; Chen, J. R.; D'Amico, K. L.; Oversluzen, T. *Rev. Sci. Instrum.* **1995**, *66*, 1812−1814.
(24) Chang, S. H.; Chang, C. H.; Juang, J. M.; Huang, L. J.; Lin, T. F.; Liu, C. Y.; et al. *Chin. J. Phys.* **2012**, *50*, 220−228.
(25) Ravel, B.; Newville, M. *J. Synchrotron Radiat.* **2005**, *12*, 537−541.
(26) Wong, J.; Lytle, F. W.; Messmer, R. P.; Maylotte, D. H. *Phys. Rev. B* **1984**, *30*, 5596−5610.
(27) Wen, Y.; Zeng, X. L.; Tong, M. Z.; Nong, F. L.; Wei, Q. W. *J. Alloys Compd.* **2006**, *416*, 206−208.
(28) Hong, J.; Wang, C. S.; Chen, X.; Upreti, S.; Whittingham, M. S. *Electrochem. Solid-State Lett.* **2009**, *12*, A33−A38.
(29) Ma, J.; Li, B.; Du, H.; Xu, C.; Kang, F. *J. Electrochem. Soc.* **2011**, *158*, A26−A32.
(30) Zhang, L. L.; Liang, G.; Ignatov, A.; Croft, M. C.; Xiong, X. Q.; Hung, I. M.; Huang, Y. H.; Hu, X. L.; Zhang, W. X.; Peng, Y. L. *J. Phys. Chem. C* **2011**, *115*, 13520−13527.
(31) Zhao, T.; Xu, W.; Ye, Q.; Cheng, J.; Zhao, H.; Wu, Z.; Xia, D.; Chua, W. *J. Synchrotron Radiat.* **2010**, *17*, 584−589.
(32) Omenya, F.; Chernova, N. A.; Upreti, S.; Zavalij, P. Y.; Nam, K. W.; Yang, X. Q.; Whittingham, M. S. *Chem. Mater.* **2011**, *23*, 4733−4740.
(33) Morgan, D.; Van der Ven, A.; Ceder, G. *Electrochem. Solid-State Lett.* **2004**, *7*, A30−A32.
(34) Kröger, F. A.; Vink, H. *J. Solid State Phys.* **1956**, *3*, 307−435.